

# THE DISTRIBUTION OF DARK MATTER IN THE HALO OF THE EARLY-TYPE GALAXY NGC 4636

DALIA CHAKRABARTY<sup>1</sup> AND SOMAK RAYCHAUDHURY<sup>2</sup>

*New manuscript: February 2, 2022*

## ABSTRACT

We present the density structure of dark matter in the outer parts (to about 7 effective radii) of the elliptical galaxy NGC 4636, from the radial velocities of 174 globular clusters, using the non-parametric, inverse algorithm CHASSIS. We find the galaxy to be rich in dark matter, with  $R$ -band mass-to-light ( $M/L$ ) ratios rising to about 30, at nearly  $4R_e$ ; the  $K$ -band  $M/L$  at about  $3R_e$  is found to be nearly 10. The result does not depend on applying the method to the red and blue globular clusters separately. This estimate of  $M/L$  is higher than the previous analysis from the same kinematic data. We also find that the dark matter distribution is highly concentrated towards the inner halo.

*Subject headings:* galaxy: kinematics and dynamics—galaxy: globular clusters: individual (NGC 4636)

## 1. INTRODUCTION

The overwhelming presence of dark matter in the outskirts of disk galaxies has been invoked to explain flat rotation curves out to several times the optical dimensions of these systems. (e.g., Roberts 1969; Faber & Gallagher 1979). However, the inferred dark matter content of cores of galaxies, in many cases, seems to fall well short of the standard model predictions (e.g., Gentile et al. 2004; Ferreras et al. 2007). In the same spirit, intriguing studies of dark haloes of early-type galaxies, using planetary nebulae as tracers of the distribution of matter, seem to indicate the under-abundance of dark matter (e.g., Romanowsky et al. 2003). This view has been challenged, however, on grounds that the subtleties in the very processing of the kinematic data can lead to spurious answers (Dekel et al. 2005; Sambhus et al. 2006; Douglas et al. 2007). In particular, the mass-anisotropy degeneracy is a difficult issue to resolve, given the limited breadth of available kinematic measurements.

In spite of this shortcoming, it is highly appealing to use kinematic information in verifying that the dark matter distribution of elliptical galaxies is in concordance with the predictions of cosmological simulations, performed within the  $\Lambda$ CDM paradigm. Globular clusters provide an independent source of test particles, since their formation histories are different from those of planetary nebulae, and the nature and distribution of their orbits would provide independent information about the distribution of the underlying dark matter. Mass modeling based on globular cluster dynamics has been tried out on nearby early-type galaxies (Côté et al. 2003; Bridges et al. 2006; Schuberth et al. 2006; Woodley et al. 2007; Hwang et al. 2008; Richtler et al. 2008), and in many cases there have been appreciable discrepancies between these results and the models obtained from planetary nebulae. Such endeavors highlight the necessity of not only studying a large number of systems for both sets of tracers, but also investigating the dependence on models, as well as trying

out different methods of mass reconstruction, in particular those that do not explicitly depend on the characterization of models.

NGC 4636 is an example of an early-type galaxy for which the different modes of mass modeling have led to a large discrepancy in the recovered mass, even at the effective radius ( $R_e=101''.7$ , Schuberth et al. 2006). NGC 4636 lies near the southern border of the Virgo cluster and is relatively isolated. It has a radial velocity similar to that of the Virgo cluster, even though it is about 3 Mpc from the center of the cluster. Furthermore, the galaxy lies at the center of a poor group (Osmond & Ponman 2004; Miles et al. 2004, 2006), possibly falling into the cluster. Its unusual properties have attracted detailed multi-wavelength research for several decades. For instance, NGC 4636 is found to be very bright in X-rays ( $L_X \sim 10^{41}$  ergs/s), with unusual features in the hot ISM (Forman et al. 1985; Matsushita et al. 1998; Jones et al. 2002; Loewenstein & Mushotzky 2003; O’Sullivan et al. 2005).

NGC 4636 has an anomalously large specific frequency of globular clusters (Dirsch et al. 2005), comparable to that of central galaxies of far richer systems, like that of NGC 1399 in Fornax (Dirsch et al. 2003). Dirsch et al. (2005) provide details of several thousand globular cluster candidates around this galaxy, of which radial velocities of 174 GCs were presented in Schuberth et al. (2006), where a dynamical analysis of this data, on the basis of Jeans Equation, was also performed, for assumed values of the stellar mass to light ratio ( $M/L$ ) and anisotropy. Naturally, the recovered mass profile is the projected one, which only provides a lower limit to the actual mass distribution. In this approach, the total mass density profile needs to be parameterized (as an NFW model, say) and constraints are recovered for these characteristic parameters. Thus, this method is not well-suited for the recovery of the distribution of total mass. Further, the estimation of the density parameters is awkwardly sensitive to the choice of the stellar  $M/L$  that is used to scale the luminosity density profile: Schuberth et al. (2006) use  $M/L$  values obtained by Bell et al. (2003), Kronawitter et al. (2000) and Loewenstein & Mushotzky (2003), from various samples of elliptical galaxies. There is of course no reason why this ratio has to be a constant and not vary with radius in the radial range covered by the kinematic

<sup>1</sup> School of Physics & Astronomy, University of Nottingham, Nottingham NG7 2RD, U.K.; dalia.chakrabarty@nottingham.ac.uk

<sup>2</sup> School of Physics & Astronomy, University of Birmingham, Birmingham B15 2TT, UK; somak@star.sr.bham.ac.uk

data (projected radius  $R \leq 30$  kpc).

According to Schuberth et al. (2006), the range of mass profiles of the halo of NGC 4636, corresponding to an assumed NFW density (Navarro et al. 1996), do indeed straddle the distribution indicated by Matsushita et al. (1998), though the profile obtained by Loewenstein & Mushotzky (2003) is found to be too massive, even for the Schuberth et al. (2006) model that corresponds to the highest dark matter content within 30 kpc.

Clearly, the use of different methods, with varying model assumptions, on different data sets, disagree in their attempts to find the underlying dark matter distribution within the same volume. Here, we take an approach which does not assume a parameterized model. We use the algorithm CHASSIS (Chakrabarty & Saha 2001) to analyze the available kinematics of the same sample of 174 GCs that is used in the Jeans Equation approach of Dirsch et al. (2005). This algorithm has been calibrated against the N-body realization of two star clusters (Chakrabarty & Portegies Zwart 2004), and applied to estimate the central mass structure of the Galaxy (Chakrabarty & Saha 2001) and the GC M15 (Chakrabarty 2006). It is also used to estimate the dark matter content in NGC 3379, using planetary nebulae kinematics (Chakrabarty 2008, in preparation).

The basic formalism of CHASSIS is discussed in the following section. Section 3 describes the observational details of the GCs used in this analysis, and in Section 4, we present the results obtained from CHASSIS for the  $M/L$  distribution in the outer parts of NGC 4636, and compare our results with previous work. Section 5 summarizes the implications of our results in the determination of the content of dark matter in the outer halo of NGC 4636.

## 2. THE CHASSIS ALGORITHM

CHASSIS works under the assumption that the input kinematic data is drawn from an equilibrium phase space distribution function that is isotropic in nature. Also, the system geometry is assumed to be spherical. The algorithm produces a pair of functions: the equilibrium phase space density and the (total) mass density, that best describe the observed data. These two characteristic functions are sought simultaneously, using a maximum likelihood approach that employs a sophisticated optimizer – the Metropolis algorithm. The inputs to the algorithm are the position on the plane of the sky, and at least one velocity component (usually the radial velocity  $v_z$ ) of individual GCs in the system.

As in all recursive algorithms, CHASSIS too requires initial guesses (or seeds) for the answers it seeks, namely the distribution function and mass density profile (represented in the code as histograms over energy and radius, respectively). The final answer should be insensitive to the choice of this guess; robustness checks are carried out to confirm this with the kinematic data used.

During any run, at the end of the first step, the seeds for the mass density and the distribution function are slightly tweaked. Likewise, at the end of subsequent step, the profiles are modified, (both in shape and overall amplitude), over their previous forms, subject to the constraints of monotonicity and positivity. This is carried on until the global maximum in the likelihood function

is identified.

The  $\pm 1\text{-}\sigma$  spread in the sample of the density and distribution functions, that correspond to the neighborhood of this global maximum, readily provides the  $1\text{-}\sigma$  error bars on the recovered profiles. Quantities that are estimated from the recovered profiles, such as the enclosed mass profile and the velocity dispersion profile, bear the signature of this extent of error. It may be noted that these errors stem from the uncertainties in identifying the global maximum in the likelihood function, and are essentially different from the observational errors. The errors in the velocity measurements are incorporated into the analysis by convolving the projected distribution function with the distribution of the observational errors, (assumed Gaussian). Further details about this algorithm can be found in Chakrabarty & Saha (2001).

CHASSIS works by projecting the distribution function in each step, at the current choice of the potential (calculated from the current choice of the mass density), into the space of observables. The product of the resulting projected distribution functions, corresponding to all the  $(r_p, v_z)$  pairs in the data set, defines the likelihood function.

## 3. DATA

The positions and radial velocities ( $v_z$ ) for the 174 globular clusters that are used in this study, (adopted from Dirsch et al. (2005)), are shown in Fig. 1. Based on surface brightness fluctuations, Tonry et al. (2001) quotes a distance to NGC 4636 to be 14.7 Mpc, while Dirsch et al. (2005) quote a distance of 17.7 Mpc based on the peak of the GC luminosity function. Both measures have considerable uncertainty, so we adopt a distance of 16 Mpc to NGC 4636, which translates to  $1'' \equiv 77.5$  pc, approximately.

As has now been found in a wide range of early-type galaxies, the colors of the GCs form a bimodal distribution, with the redder, more metal-rich GCs more likely to harbor low-mass X-ray binaries (e.g. Jordán 2004; Posson-Brown et al. 2006; Kundu & Zepf 2007; Woodley et al. 2008), there being significant differences in key structural as well as chemical properties in the two populations (e.g. Jordán et al. 2007). According to the photometry of Dirsch et al. (2005), the blue and red GCs of NGC 4636 can be characterized as  $C - R$  color being greater than or less than 1.55 respectively. We show this classification in the left panel of Figure 1. Another way of classifying the data at hand is along the lines of the magnitude of the measured velocity errors; any GC with a measurement error exceeding  $35 \text{ km s}^{-1}$  is assigned to one kinematic class while those with higher velocity errors for the other group. We carry out runs with all GCs, and separately with the sub-samples that characterize each of these photometric and kinematic classes.

The right panel of Fig. 1 shows the spatial distribution of the globular clusters used in this study. This is a small fraction of the GC candidates of Dirsch et al. (2005), and represents the clusters that Schuberth et al. (2006) report as belonging to the galaxy, on the basis of spectroscopic data. As is apparent from this picture, the number of observed GCs decreases rapidly beyond about 30 kpc, and beyond 50 kpc, there are only 2 velocity measurements available. This radial profile of the measured data set is important in determining the choice

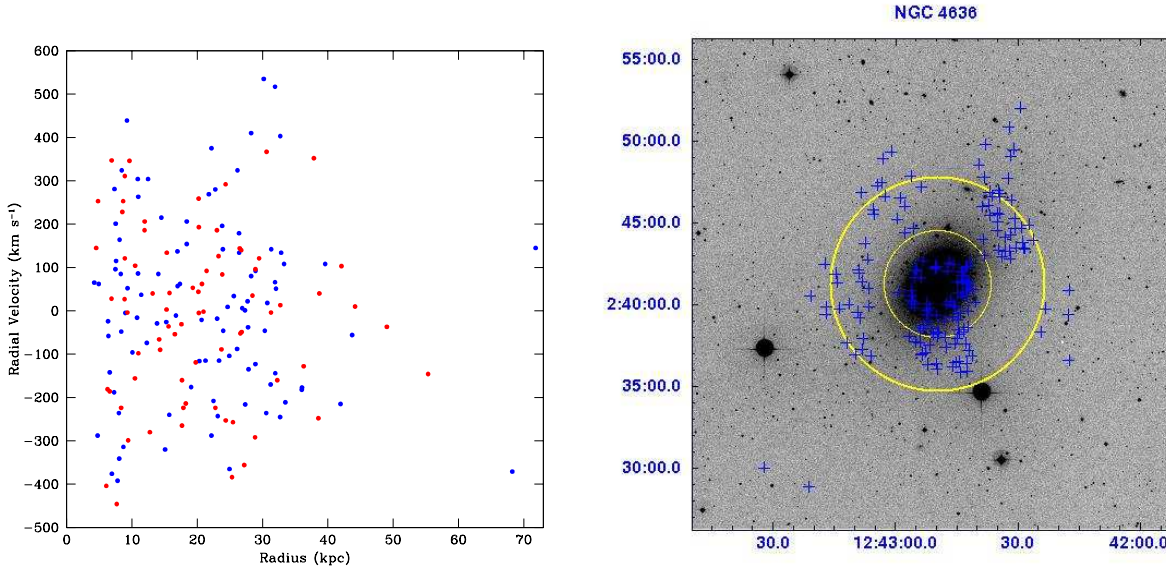


FIG. 1.— Left: Measured radial velocities of the globular clusters of NGC 4636 used in this analysis, as a function of projected distance from the center of the galaxy. The red points represent the 76 red GCs ( $C-R$  color  $> 1.55$ ), while the blue points the 98 blue GCs ( $C-R \leq 1.55$ ). Right: The distribution of these GCs (blue crosses) on the sky, superposed on an optical DSS image of NGC 4636. The two yellow circles correspond to radii of 15 and 30 kpc respectively.

of the radial binning adopted in this analysis.

For the application of CHASSIS, the radial bin width needs to be such that the left edge of the innermost bin must not exceed the smallest projected radius at which the radial velocity data is available. Working with too small bin widths would lead to bins that contain no velocity information at small radii. On the contrary, adopting too large a bin width can lead to spurious density profiles, especially nearer to the center of the system, where the gradient in density is higher than in the outer parts. Given these constraints, we experimented with bin sizes and found that a choice of 2 kpc is adequate for this data set. This value allows us to span radial distances over a range of 4.2 kpc to about 55 kpc. However, the results recovered by CHASSIS are not crucially sensitive to the exact choice of the bin width; this feature of the code will be demonstrated below with results from experiments done with assorted bin width values.

The 3-D total mass density that is recovered by CHASSIS is then used to calculate the enclosed mass profile which is subsequently compared to the cumulative light profile, in order to extract the mass-to-light ratio ( $M/L$ ) profile. In this context, we use the  $K$ -band surface brightness profile of NGC 4636, obtained from the photometry of the 2MASS large galaxy Atlas (Jarrett et al. 2003), kindly provided to us by Tom Jarrett. This is shown in red in the left panel of Fig. 2). We deproject this under the assumption of spherical symmetry (right panel of Fig. 2) with a non-parametric deprojection code DOPING (Chakrabarty & Ferraese 2008). We also use the  $R$ -band photometry from Dirsch et al. (2005) to estimate the  $M/L$  profile in the  $R$ -band.

#### 4. RESULTS

To begin with, the insensitivity of the results to the choice of the first guess for the distribution function needs to be established. For this purpose, we undertake to parameterize the seed for the density by an NFW-like

profile (Navarro et al. 1996):

$$\rho(r) = \frac{\rho_0}{(r/r_c)^\alpha (1 + r/r_c)^2}. \quad (1)$$

The phase space distribution function is either held as a power-law (with a power-law index of  $\beta$ ) or as an exponential of the effective energy ( $\epsilon$ ). Thus, the seed for the density distribution is characterized by a total of 3 parameters, namely  $\rho_0$ ,  $r_c$ ,  $\alpha$ , out of which, the amplitude or the central density parameter  $\rho_0$  is found to have no effect whatsoever on the result. Three different seeds characterized by the form of the DF and values of  $r_c$ ,  $\alpha$ , were implemented in three distinct runs:

- RUN I – the seed distribution function is set to  $\exp(\epsilon)$ ,  $r_c=50$  kpc and  $\alpha=2.8$ ; kinematic data of all 174 GCs are used.
- RUN II – the seed distribution function  $\propto \epsilon^2$ ,  $r_c=5$  kpc and  $\alpha=1.8$ ; all GCs are used.
- RUN III – the seed distribution function is  $\propto \epsilon$ ,  $r_c=15$  kpc and  $\alpha=2.3$ ; again, the whole sample is used.

The density profiles resulting from these three runs are shown in the lower left panel of Fig. 3. As indicated by the results from the different runs, the recovered density profiles overlap within the error bars, at almost all radii. This lends confidence in the functionality of CHASSIS. The estimated density profiles are then used to calculate the enclosed mass distributions from which (lower right in Fig. 3), the radial distributions of  $M/L$  are recovered in the  $R$  and  $K$  bands (upper left Fig. 3). Since the  $K$ -band photometry is available to about 23.5 kpc, the run of  $M/L$  is also displayed till this radius, while the  $R$ -band  $M/L$  is limited to 30 kpc. As expected from a typical color of an early-type galaxy, the lower limit on the ratio between the  $R$ -band and  $K$ -band  $M/L$  values, at 20 kpc, is about 2.5. The DF recovered from

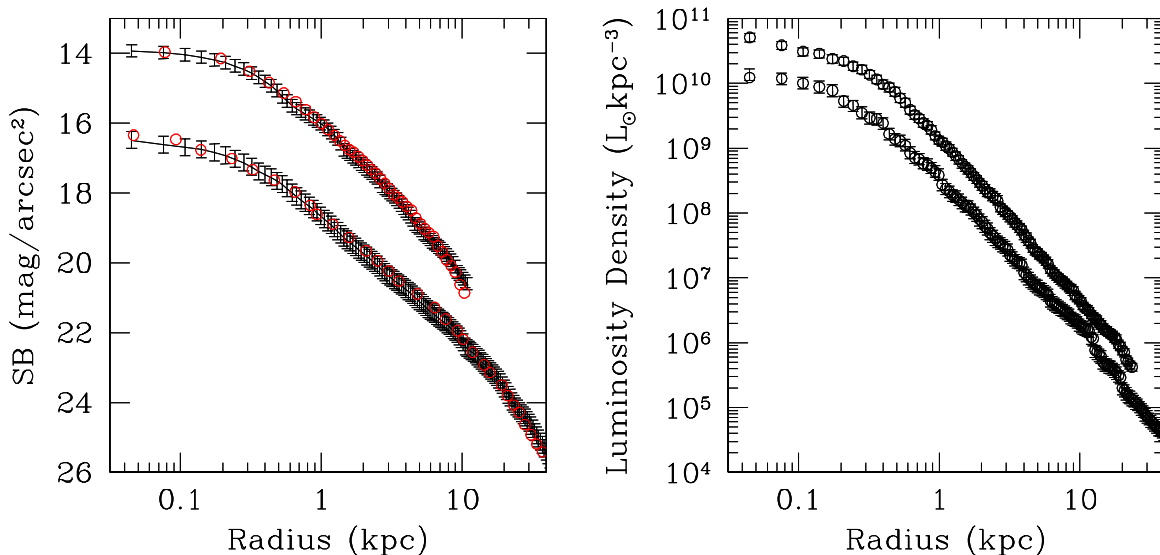


FIG. 2.— The  $R$ -band (lower curve; from Dirsch et. al 2005) and  $K$ -band (upper curve; 2MASS, Jarrett et al. (2003)) surface brightness profiles of NGC 4636 along the major axis, are shown in red on the left. The deprojected luminosity density profiles (upper curve for  $K$ -band and lower curve for  $R$ -band) are shown on the right and the projections of the same have been overlaid in black over the brightness profiles, in the left panel. The deprojection was carried out assuming that the intrinsic geometry of the tracer population is spherical.

three of the runs is used to calculate the velocity dispersion along the line-of-sight. These have been represented in the upper right in Fig. 3. (It is worth pointing out here that in the analysis of Chandra and XMM-Newton observations (O’Sullivan et al. 2005), it has been found that between 25–30 kpc, there is an abrupt transition between the hot interstellar medium of the galaxy to the intergalactic medium of the surrounding group). The robustness of the algorithm to the choice of bin width is displayed in Figure 4.

To confirm that the results of RUN I, RUN II and RUN III are not artifacts of the details of the sampling of the tracer population, we performed individual runs with sub-samples that correspond to different GC color and (radial velocity) measurement accuracy classes. These runs are described below:

- RUN IV - the seed distribution function is set to the same as for RUN I; kinematic data of the 76 red GCs are used.
- RUN V - the seed is as in RUN I; the 98 blue GCs are used.
- RUN VI - again, the seed is identical to that used in RUN I; implemented velocity data are that of the 121 GCs (red *and* blue) that have velocity errors lower than a cutoff of  $35 \text{ km s}^{-1}$  (Schuberth et al. 2006).

These three runs are carried out with bin widths of 2 kpc. The size of the error bars on the recovered DF and density distributions will be higher for these runs than for RUNS I, II and III, which employ the whole sample, i.e. a greater number of data points. The results are shown in Fig. 5.

It is notable that the division of the whole sample of the GCs by color did not yield significantly different total mass densities; there is indeed a trend for the bluer GCs in the sample to be on the higher side of the mass of the redder GCs, but as is apparent from Fig. 5, the distinction in the recovered mass profile is not strong enough

to be deemed significant, at  $\pm 1\text{-}\sigma$  level. The effect of division by kinematic accuracy is even less potent.

Thus, it appears that the  $M/L_K$  distribution within the first three effective radii, can at most be about 12 in the  $K$ -band, when the errors of the deprojection, as performed by DOPING are ignored; when the errors of the deprojection are included, the range of the  $M/L$  value recovered at about 23.5 kpc ( $\approx R_e$ ) is found to widen to about 8 to 14.

#### 4.1. Effect of Assumptions on Mass Recovery

Within CHASSIS, the effect of imposing isotropy in velocity space, where anisotropy prevails, is to recover spuriously high mass density values (Chakrabarty 2006). Though in general it is difficult to quantify the extent of this bias since it depends on the structure of the unknown distribution function, in the case of NGC 4636, we can surmise that the effect of anisotropy is not significant at the  $1\text{-}\sigma$  level. We infer this using the following result that Schuberth et al. (2006) report: it is the red sub-sample of the observed GCs that were found to exhibit “significant rotation” in contrast to the blue GCs which do not show a “significant signal”. However, from Figure 5 we see that the mass density profiles that we recover for the red and blue sub-samples are consistent with each other within the error bars (though the density distribution of the red GCs is on the higher side).

As for the deviation from sphericity is concerned, Schuberth et al. (2006) suggest an ellipticity of 0.15 for NGC 4636. This is in reference to the photometric appearance of the galaxy while observational constraints on the spatial distribution of the dark matter halo of the galaxy, within which the globular cluster system resides, is harder to come by<sup>3</sup>. Schuberth et al. (2006) treat NGC 4636 as spherical, motivated by the confirmation of “modest” deviations from sphericity in the inner parts of the galaxy (courtesy Dirsch et. al 2005), where most of the GCs live.

However, it needs to be appreciated that in CHASSIS, the assumption of sphericity pertains to the geometry

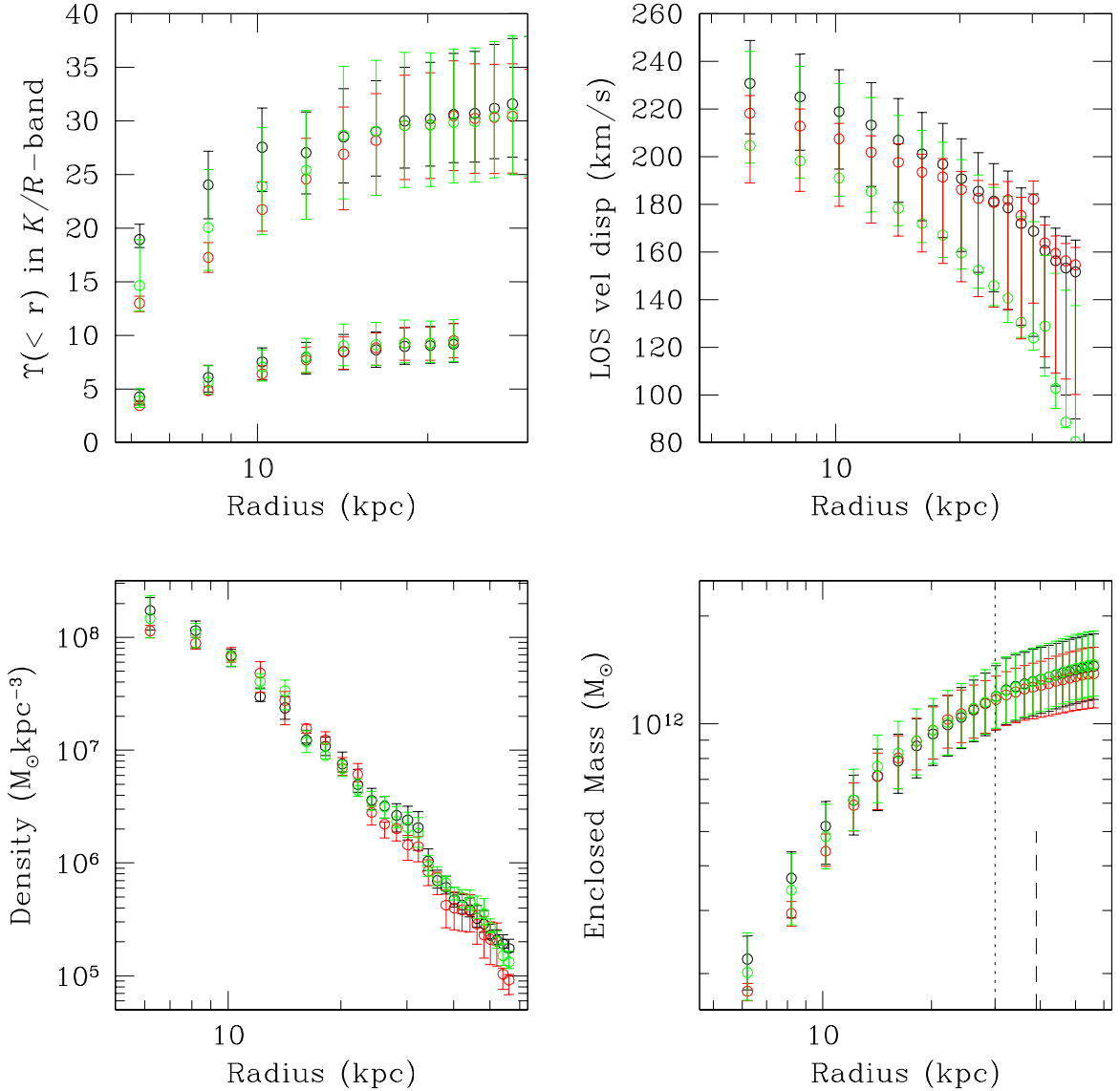


FIG. 3.— *Lower left:* The recovered 3-D total (dark+luminous) density profiles of NGC 4636, to about 7 times the effective radius (which is  $101''.7 \approx 7.8$  kpc), from three different runs, that were performed with distinct forms of the initial guesses (seeds) for the DF and mass density distributions. Results for RUN I are in black, RUN II in red and RUN III in green (details in §4). *Lower right:* Enclosed mass profiles from the density distributions recovered from these runs. The dotted line in black represents 30 kpc, the radius at which the mass predicted by CHASSIS is compared to the mass estimates from other work. The dashed line represents the  $5R_e$  mark. *Upper left:* The  $K$ -band (lower curve) and  $R$ -band (upper curve) mass-to-light ratios in the outer parts of NGC 4636. Note that the  $M/L$  distributions in this figure do not include the uncertainties involved in the deprojection of the observed brightness profile into the intrinsic luminosity profile, in order to represent the extent of the errors in the analysis due to CHASSIS alone; allowing for these errors would widen the range of  $\Upsilon_K$  at about 24 kpc (edge of the available photometry) from about 9–12 to about 8–14. The quality of the  $R$ -band photometry implied truncating the  $M/L_R$  estimate to within 30 kpc even though mass estimates are available to larger distances. *Upper right:* The velocity dispersion along the line-of-sight, estimated from the isotropic equilibrium distribution function recovered by CHASSIS, from the runs RUN I, RUN II and RUN III.

of the total gravitational potential that the set of test particles sit in, rather than to the spatial distribution of the test particles. Thus, we assume that it is the outer parts of NGC 4636 (including its dark halo) that is spherical. In any case, mistaking an ellipsoidal system as spherical will imply overestimation of the enclosed mass profile that is calculated from the recovered mass density distribution. Erroneous formulation of the potential will also add uncertainty to the recovery of the mass density distribution itself though seeking to quantify this bias is again not direct, given that it depends on the very unknown that we are trying to constrain, namely the

mass distribution in this system.

#### 4.2. Comparison with Other Work

The hot X-ray emitting interstellar medium (ISM) has been well-studied (Jones et al. 2002; Loewenstein & Mushotzky 2003; O’Sullivan et al. 2005), with the deepest observations going out to about 30 kpc which is a radial extent that is well sampled by the GCs used in this analysis. Matsushita et al.

<sup>3</sup> The globular cluster system in M87 was reported to be elliptical in projection (McLaughlin et al. 1994), though Côté et al. (2001) approximate the 3-D spatial distribution of this system as spherical.



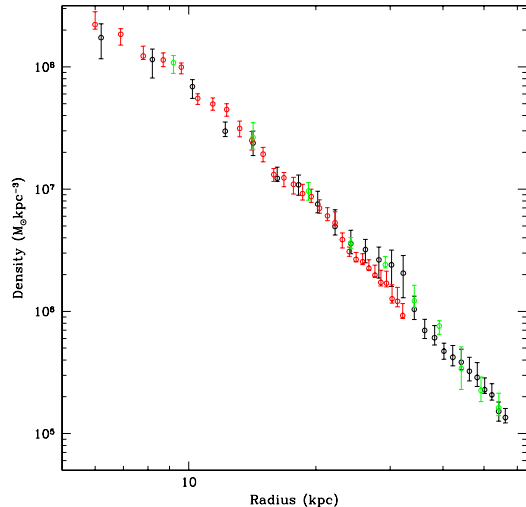


FIG. 4.— This shows the concordance (within  $\pm 1\text{-}\sigma$  error bars) of density profiles recovered from runs performed with initial conditions corresponding to RUN 1 and bin widths of 2 kpc (in black), 1 kpc (in red) and 5 kpc (in green). The unavailability of kinematic information in 1 kpc sized bins, beyond about 30 kpc, limits the radial range over which the density can be sought in this case.

(1998) and Loewenstein & Mushotzky (2003) concluded that NGC 4636 is an extremely dark matter dominated galaxy, on the basis of their analysis of ASCA and Chandra X-ray observations respectively, by fitting hot plasma models and assuming hydrostatic equilibrium. When compared carefully, their mass profiles appear to be significantly different from each other - the enclosed mass profile of Matsushita et al. (1998) flattens out beyond 10 kpc, reaching  $5 \times 10^{11} M_\odot$  at 30 Kpc, while the Loewenstein & Mushotzky (2003) profile rises steadily to beyond  $10^{12} M_\odot$  at the same distance.

However, as is seen from the detailed analysis of the Chandra and XMM-Newton observations by Jones et al. (2002) and O’Sullivan et al. (2005), the hot gas has large-scale arm like features that are indicative of AGN outburst, and thus the equilibrium assumption might not be a good one. These observations also indicate that at about 30 kpc, there is an abrupt transition of the hot interstellar medium of the galaxy NGC 4636 to the intra-cluster medium of the group surrounding it, where the gas is of significantly lower temperature and abundance. From these observations, it is hard to decouple the dark matter halo of the surrounding group from the dark halo of the galaxy itself, but inner to 30 kpc, the dark halo of the galaxy must dominate.

In terms of the shape of the predicted mass profiles, we find that unlike the mass profiles of Matsushita et al. (1998), (which exhibit a distinct flattening outside an intermediate radius of  $\sim 10$  kpc), our cumulative mass profiles do not indicate any sharp flattening - instead, the slope of the profile gradually tapers off from about 10 kpc, such that even at about 50 kpc, it is only slightly rising.

This is similar in nature to the mass profile obtained by Schubert et al. (2006) from their Model 14, i.e. their model with the highest enclosed mass within 30 kpc. In fact, Schubert et al. (2006) speculate that the flattening observed by Matsushita et al. (1998) could be a peculiar-

ity of the ASCA data itself. In any case, the apparent lack of hydrostatic equilibrium indicates that X-ray derived mass profiles might not be reliable. This may explain why our estimate of the mass of NGC 4636 falls short of what Loewenstein & Mushotzky (2003) suggest on the basis of their X-ray studies.

The mass profiles inferred from a Jeans analysis of the GC kinematics (Schubert et al. 2006) also yield high values of the dark matter content in this region - the highest and lowest values from their models yield a cumulative mass of  $0.5\text{--}0.95 \times 10^{12} M_\odot$  at 30 kpc. At the error level of  $+1\text{-}\sigma$ , our recovered mass at about 30 kpc is in excess of that suggested by the Schubert et al. (2006) analysis, from the same observational data, the lowest range of our errors being just about consistent with the highest range obtained by them. Here we recall that over-estimation of mass density, at radii where velocity anisotropy is present, is expected to be an artifact of the assumption of isotropy (though as discussed in Section 4.1, the effect of this artifact is not expected to be significant). Thus, the mass-to-light ratios presented in this paper are expected to be on the higher side of the true values in the two bands discussed ( $K$  and  $R$ ). The recovered velocity dispersion profile embraces the dispersion values depicted by Schubert et al. (2006), within the  $\pm 1\text{-}\sigma$  error bars.

It needs to be appreciated that our work is not reliant on photometry for the extraction of the all important total mass density of the system, and thus we are able to offer mass estimates much further into the halo of NGC 4636, than any of the earlier attempts. We can, in fact, calculate the mass density to just inside  $7R_e$ . Of course, the computation of the  $M/L$  profiles is constrained by the limitations of photometry.

## 5. DISCUSSION: DARK MATTER IN THE HALO OF NGC 4636

We compute the circular velocity profile of the GC system of NGC 4636 to understand the distribution of dark matter in this system. This  $v_c$  profile is shown in black, as a function of radius in the left panel of Figure 6. The profile in red is given as the function  $\sqrt{GM_{3R_e}/r}$ , where  $G$  is the universal gravitational constant and  $M_{3R_e}$  is the mass that is enclosed within 3 effective radii. Thus, the function plotted in red merely exhibits a Keplerian  $r^{-1/2}$  fall-off with radius. The errors on this function are the  $\pm 1 - \sigma$  errors on  $M_{3R_e}$ , as recovered by CHASSIS.

As is apparent from this figure, there is no significant difference between the black and red profiles to about 45 kpc. This indicates that the dark halo contribution to the mass, in the radial range  $3R_e$  to about  $5.8R_e$  is not significantly different from the mass at  $3R_e$ . This lower radius would be normally expected to bear a lower dark matter contribution than the part of the galaxy outside  $5R_e$ . That this expected trend is not statistically valid for the case of NGC 4636, can be interpreted to conclude that the distribution of mass in the dark halo of this galaxy is highly concentrated. This explanation suggests itself readily, since the prospect of low dark mass content can be ruled out on the basis of the very high  $M/L$  ratio values that we have recovered.

Driven by this hunch, we proceeded to fit an NFW density distribution (Navarro et al. 1996) to the density

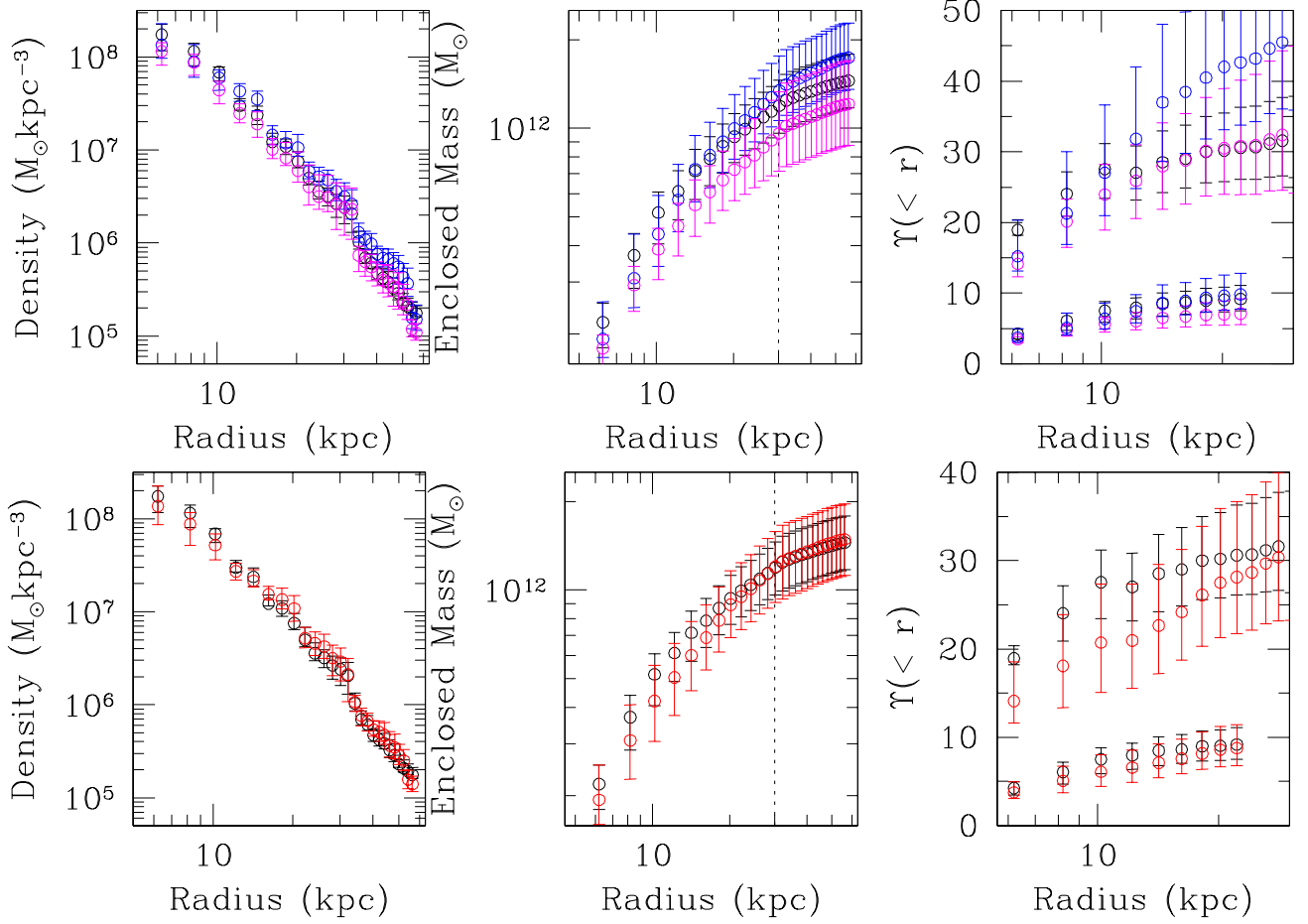


FIG. 5.— *Top Panel:* Total mass density, enclosed mass and  $M/L$  in the  $R$  (upper curve) and  $K$ -band (lower curve), from kinematic data of all clusters (RUN I, in black), red GCs (RUN IV, in pink) and blue GCs (RUN V, in blue). *Bottom Panel:* Total mass density, enclosed mass and  $M/L$  in the  $R$  (upper curve) and  $K$ -bands (lower curve) from kinematic data of all clusters (RUN I, in black) and the GCs with the relatively better kinematic accuracy (RUN VI, in red).

that is recovered by CHASSIS, from one of the presented runs (say, RUN I). Of course, this fit is non-trivial and depends on the radial range in the data over which the fit is sought. We performed a recursive routine to constrain the mass ( $M_s$ ) and length scales ( $r_s$ ) in the NFW form, such that the extracted  $r_s$  lay within the radial range under consideration. The iterations were carried out till convergence was spotted within the errors of the fit, which were high. The radial range over which the fit was sought extended from  $4R_e$  to about  $7R_e$  while the values of  $r_s$  and  $M_s$  were recovered to be  $33.7 \text{ kpc} \pm 11\%$  and about  $1.7 \times 10^{12} M_\odot \pm 8\%$ , respectively. This fit is shown, superimposed in red, on the recovered density (in black), in the right panel of Figure 6. This recovered  $r_s$  would indicate a very high concentration of at least 9, for an assumed  $M_{200}$  of at least  $2 \times 10^{12} M_\odot$ . This is indicative of a strongly concentrated system.

Lintott et al. (2006) have found that in a sample of about 2000 ellipticals from the Sloan Digital Sky Survey, the distribution of  $c$  is log-normal, with the peak lying in the range of 3-10. Thus, on this scale, the dark halo of NGC 4636 is predicted to be very highly concentrated indeed!

Recently, Napolitano et al. (2007) have suggested a di-

chotomy in the dark matter distribution of nearby early-type galaxies (probed by the Planetary Nebula Spectrograph), where one class (the “ordinary”, fast-rotating, discy/cuspy, early type systems) exhibit rapidly dropping velocity curves while the other slowly rotating, boxy/cored systems display flatter trends in their rotation curves. From Figure 6 we can see that the medial value of the circular velocity increases from about  $400 \text{ km s}^{-1}$  to an intermediate peak of about  $450 \text{ km s}^{-1}$ , to drop to around  $400 \text{ km s}^{-1}$  again, at  $5R_e$ . Thus, the rotation curve of this galaxy does not display the kind of “pseudo-Keplerian” fall-off of the that Napolitano et al. (2007) identify with the “ordinary” class of ellipticals. Thus, our interpretation of NGC 4636 as a dark-matter rich galaxy is consistent with the latter class of galaxies.

#### ACKNOWLEDGMENTS

We thank Tom Jarrett for supplying us with unpublished 2Mass photometry for the  $K$ -band surface brightness profile, and Mike Merrifield for very useful discussions. Thanks to Ylva Schuberth for sharing observational results with us before publication. DC is funded by a Royal Society Dorothy Hodgkin Fellowship.

#### REFERENCES

Bell, E. F., McIntosh, D. H., Katz, N., & Weinberg, M. D. 2003, *ApJS*, 149, 289

Bridges, T., et al. 2006, *MNRAS*, 373, 157

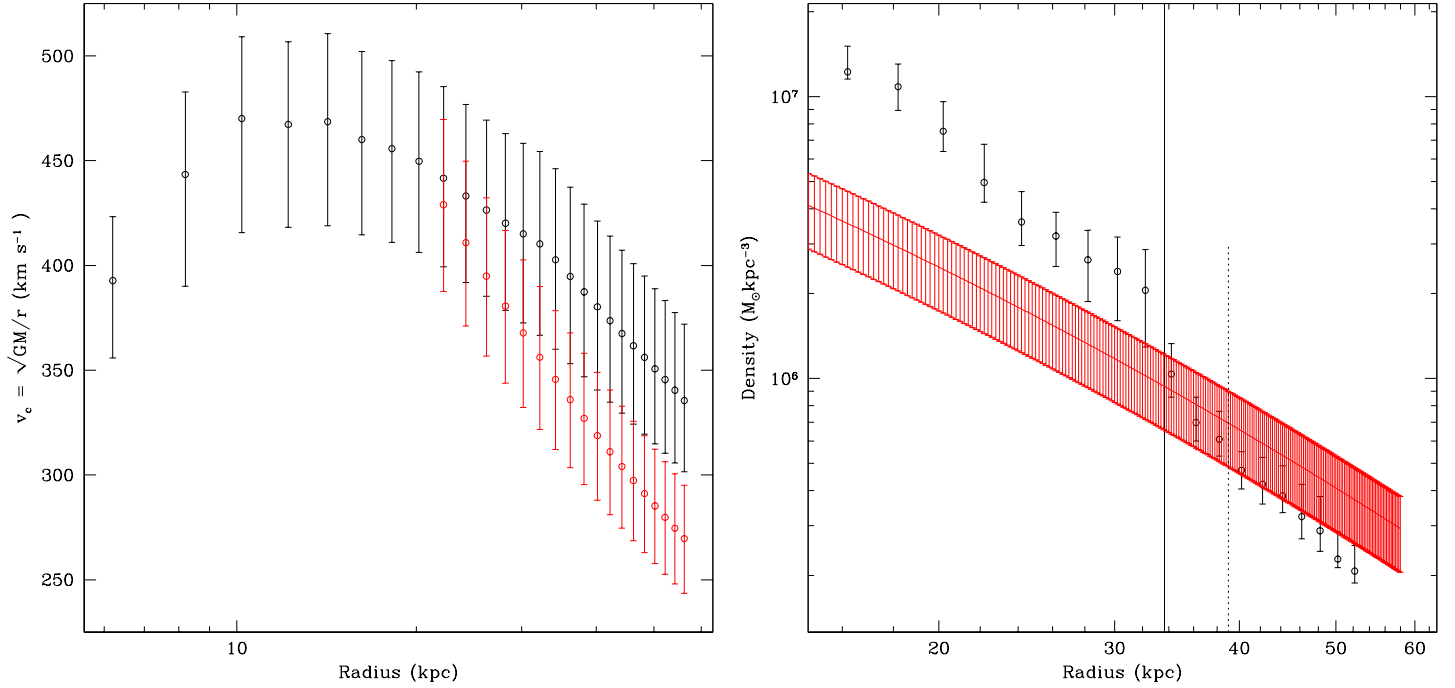


FIG. 6.— The left panel shows the circular velocity curve of NGC 4636, as recovered from RUN I. The function in red represents the Keplerian fall-off with radius, normalized by  $\sqrt{GM_{3R_e}}$ , where  $M_{3R_e}$  is the mass found to be enclosed within  $3R_e$ . The errors on the red profile are the  $\pm 1\text{-}\sigma$  errors in the value of  $M_{3R_e}$ , as indicated by the algorithm. The right panel shows an NFW fit (in red) to the total mass density recovered from RUN I (in black). The errors of the fitting procedure define the error band shown in red. The solid line represents the inner edge of the radial range over which the fit is sought. The dotted line indicates  $5R_e$ .

Chakrabarty, D., & Portegies Zwart, S. 2004, *AJ*, 128, 1046  
 Chakrabarty, D., & Saha, P. 2001, *AJ*, 122, 232  
 Chakrabarty, D. 2006, *AJ*, 131, 2561  
 Côté, P., McLaughlin, D. E., Cohen, J. G., & Blakeslee, J. P. 2003, *ApJ*, 591, 850  
 Côté, P., et al. 2001, *ApJ*, 559, 828  
 Dekel, A., Stoehr, F., Mamon, G. A., Cox, T. J., Novak, G. S., & Primack, J. R. 2005, *Nature*, 437, 707  
 Dirsch, B., Richtler, T., Geisler, D., Forte, J. C., Bassino, L. P., & Gieren, W. P. 2003, *AJ*, 125, 1908  
 Dirsch, B., Schuberth, Y., & Richtler, T. 2005, *A&A*, 433, 43  
 Chakrabarty, D. & Ferrarese, L., 2008, *International Journal of Modern Physics D*, as part of proceedings for the 6th International Workshop on Data Analysis in Astronomy, "Modelling and Simulations in Science", Vol 17, No 2.  
 Douglas, N. G., et al. 2007, *ApJ*, 664, 257  
 Faber S. M., Gallagher J. S., 1979, *ARA&A*, 17, 135  
 Ferreras I., Saha P., Williams L. L. R., Burles S., 2007, arXiv, 708, arXiv:0708.2151  
 Forman, W., Jones, C., & Tucker, W. 1985, *ApJ*, 293, 102  
 Hwang, H. S., et al. 2007, ArXiv e-prints, 709, arXiv:0709.4309  
 Jarrett, T. H., Chester, T., Cutri, R., Schneider, S. E., & Huchra, J. P. 2003, *AJ*, 125, 525  
 Jones, C., Forman, W., Vikhlinin, A., Markevitch, M., David, L., Warmflash, A., Murray, S., & Nulsen, P. E. J. 2002, *ApJ*, 567, L115  
 Jordán, A., et al. 2007, *ApJ*, 671, L117  
 Jordán, A. 2004, *ApJ*, 613, L117  
 Kronawitter, A., Saglia, R. P., Gerhard, O., & Bender, R. 2000, *A&AS*, 144, 53  
 Kundu, A., & Zepf, S. E. 2007, *ApJ*, 660, L109  
 Lintott, C. J., Ferreras, I., & Lahav, O. 2006, *ApJ*, 648, 826  
 Loewenstein, M., & Mushotzky, R. 2003, *Nuclear Physics B Proceedings Supplements*, 124, 91  
 Mamon G. A., Lokas E. L., 2005, *MNRAS*, 363, 705  
 Matsushita, K., Makishima, K., Ikebe, Y., Rokutanda, E., Yamasaki, N., & Ohashi, T. 1998, *ApJ*, 499, L13

Miles, T. A., Raychaudhury, S., & Russell, P. A. 2006, *MNRAS*, 373, 1461  
 Miles, T. A., Raychaudhury, S., Forbes, D. A., Goudfrooij, P., Ponman, T. J., & Kozhurina-Platais, V. 2004, *MNRAS*, 355, 785  
 Napolitano, N. R., et al. 2007, ArXiv e-prints, 709, arXiv:0709.1636  
 Osmond, J. P. F., & Ponman, T. J. 2004, *MNRAS*, 350, 1511  
 O'Sullivan, E., Vrtilek, J. M., & Kempner, J. C. 2005, *ApJ*, 624, L77  
 Posson-Brown, J., Raychaudhury, S., Forman, W., Hank Donnelly, R., & Jones, C. 2006, ArXiv Astrophysics e-prints, arXiv:astro-ph/0605308  
 Richtler, T., Schuberth, Y., Hilker, M., Dirsch, B., Bassino, L., & Romanowsky, A. J. 2008, *A&A*, 478, L23  
 Roberts M. S., 1969, *AJ*, 74, 859  
 Gentile G., Salucci P., Klein U., Vergani D., Kalberla P., 2004, *MNRAS*, 351, 903  
 McLaughlin, D. E., Harris, W. E., & Hanes, D. A. 1994, *ApJ*, 422, 486  
 Navarro, J. F., Frenk, C. S., & White, S. D. M. 1996, *ApJ*, 462, 563  
 Romanowsky A. J., Douglas N. G., Arnaboldi M., Kuijken K., Merrifield M. R., Napolitano N. R., Capaccioli M., Freeman K. C., 2003, *Sci*, 301, 1696  
 Sambhus, N., Gerhard, O., & Méndez, R. H. 2006, *AJ*, 131, 837  
 Sambhus, N., Gerhard, O., & Méndez, R. H. 2005, AIP Conf. Proc. 804: Planetary Nebulae as Astronomical Tools  
 Schuberth, Y., Richtler, T., Dirsch, B., Hilker, M., Larsen, S. S., Kissler-Patig, M., & Mebold, U. 2006, *A&A*, 459, 391  
 Tonry, J. L., Dressler, A., Blakeslee, J. P., Ajhar, E. A., Fletcher, A. B., Luppino, G. A., Metzger, M. R., & Moore, C. B. 2001, *ApJ*, 546, 681  
 Woodley, K. A., et al. 2008, ArXiv e-prints, 801, arXiv:0801.1640  
 Woodley K. A., Harris W. E., Beasley M. A., Peng E. W., Bridges T. J., Forbes D. A., Harris G. L. H., 2007, *AJ*, 134, 494